Three Dimensional Cellular Structures Enhanced By Shape Memory Alloys

Principal Investigator: Michael V. Nathal, GRC/Advanced Metallics Branch
David Krause, Nathan Wilmoth, Eric Baker and Brett Bednarcyk, GRC/Mechanics and Life Prediction Branch; Santo Padula, GRC/Advanced Metallics Branch

Summary

This proposal seeks to explore and develop lightweight structural concepts married with advanced "smart" materials to achieve a wide variety of benefits in airframe and engine components. In this first year effort, we developed and assembled the methods to address the key aspects of these structures, including structural testing and modeling. The test results demonstrated good structural performance, validated the deformation models, and demonstrated shape memory behavior in the cast lattices.

Introduction

The technical literature abounds with lightweight structural concepts using periodic cellular structures such as honeycombs and lattice block materials. Honeycombs have been primarily used in lightweight sandwich structures and are some of the most efficient (strength/density) structures in many important loading situations such as bending. Lattice block, consisting of truss architectures at a micro-or meso-scale, are preferred over honeycombs when the loading situations are more three dimensional, or when honeycomb fabrication is not compatible with the desired material selection. In the past 5 years, an exciting outgrowth of these concepts is the development of "auxetic" structures, which are characterized by negative Poisson's ratios (indicating that a material/structure gets thicker when it is stretched, the opposite of normal behavior). The combination of strength and flexibility of these structures enable many innovative lightweight structural concepts such as morphing wings and fan blades, and auxetics are also projected to have improved impact resistance and therefore have relevance to fan containment systems. Constructing the cellular structures from shape memory alloys (SMAs) provides even greater potential. SMAs can be used in two ways, depending on alloy selection and temperature. First, SMAs can be designed to take advantage of the shape memory effect. Here, the structure can change shape as a response to heating and cooling cycles to achieve morphing behavior, or alternately a self-healing concept where damage from an impact event can be recovered via a thermal treatment. Secondly, SMAs can be designed to be superelastic, where extremely high deformations and loads can be achieved while still behaving in a reversible manner similar to an elastic response (and thereby allowing long lives and durability in fatigue, gust and impact loading situations).

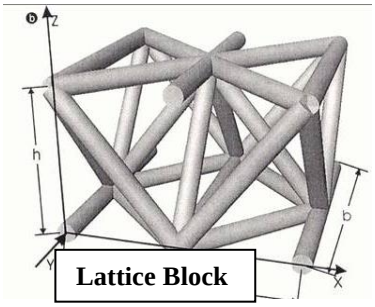

Lattice Block

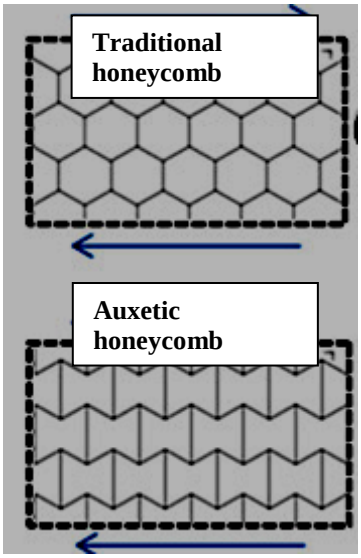

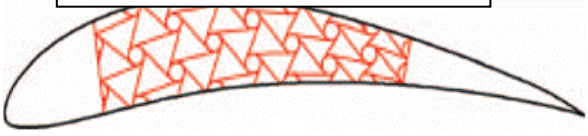
Auxetic morphing airfoil from Spadoni et al. 2005

The number of materials that can actually be made into these cellular structures has been limited to some plastics and a few relatively soft metallic alloys. Thus, most of these morphing concepts remain as computer models or as simple benchtop models. We

have attempted to improve the aerospace relevance of these structures by active engagement with outside companies to develop manufacturing methods via SBIR awards. Our collaboration with T45 Inc., through a Phase II SBIR effort (initiated in July 2011 and still continuing), has demonstrated the initial manufacturing feasibility of SMA lattice blocks, titanium auxetics and SMA auxetics. Application of these SMA-based structural concepts and exploiting their unique properties will require detailed understanding of mechanical properties and deformation behavior under cycling conditions, which are beyond the scope of the SBIR contract with T45, and is the focus of the ARMD Seedling Fund effort. Our concept is to apply SMAs to lattice and auxetic structures that will expand capabilities into three dimensional actuation, new lightweight and flexible flap and winglet designs, variable geometry inlets and nozzles, as well as highly-impact resistant structures. Although our primary goal is to demonstrate performance of SMA-based lattice block and auxetic structures, we included Ti-6-4 to serve as a baseline for comparison to the SMAs, and as a lower risk material to demonstrate the lattice technologies. In addition, Ti-6-4 auxetics offer substantial benefits by themselves.

Potential impact on NASA and national aeronautics challenges

NASA subsonic and supersonic programs have N+2 and N+3 goals for fuel efficiency and noise that can be met be utilizing innovative lightweight structural concepts such as morphing wings, inlets, nozzles and fan blades. The current SFW and SUP projects are funding improved SMA alloy development and simple one-dimensional SMA actuation concepts, such as wires pulling on a lever, or a tube rotating a flap. These SMA-based concepts provide substantial weight savings over state-of-the-art actuation systems, and are frequently enabling. Even greater benefits can be achieved, and even more components can be available for morphing designs via integrating these three dimensional structures. The benefits of auxetic structures, as well as any superelastic structure, are too new to have been fully explored. Improved morphing capacity, improved structural optimization, improved gust load alleviation, and improved impact resistance are all envisioned.

It is expected that successful demonstration of properties and conceptual design will lead to further development in the SFW and/or SUP projects [Note: currently all SUP work on SMAs is being transferred to the new Aero Sciences project]. Lattice structure optimization will be the initial focus of the FAP task, along with incorporation of NASA-developed SMA's with higher temperature or higher actuation performance as well. This will be followed by component demonstrations. The potential for a separate entry into a fan containment project is also possible, with either the Ti alloy or an SMA. Successful demonstration of the technology at TRL= 3 can also result in transition of the technology to ERA – Phase III.

PHASE I PROGRESS REPORT

The objectives of Phase I were to demonstrate shape memory behavior in both lattice and auxetic structures and compare the results with a more conventional aerospace Ti alloy as a baseline. This demonstration was to be supported by testing and modeling tasks to provide the understanding required for future design and optimization efforts.

1. Material Processing

The number of lattice castings supplied by T45 was less than originally planned for two reasons. First, there was a considerable delay in the SBIR Phase II program, which delayed all Phase II contracts by roughly 5 months. Second, there were technical issues related to a higher incidence of casting defects. This resulted in T45 delaying delivery of the original planned castings until it could deliver higher quality castings. Most of the SMA castings as well as all of the auxetic castings we were expecting in March, 2012 have yet to be delivered. The SMA castings that we did receive have a higher population of casting defects than T45 would normally deliver, but we elected to receive these in order to get at least a preliminary indication of SMA lattice behavior. Cracks were the most

significant defect, and occurred particularly at lattice nodes. The particular composition for this work, Ni-50at% Ti, was chosen because of its very high shape memory actuation capacity. However, this alloy is not optimally processed by casting, and substantial amounts of the deleterious Ti_2Ni phase were found during microscopic characterization of the castings. Attempts to minimize this embrittling phase by modifying the casting parameters are in progress. If these trials are unsuccessful, a new Ni-rich alloy (Ni-49.8at % Ti) may be the best choice for future castings. Defects were present in the Ti-6-4 castings also, but at a much lower frequency than the SMA castings. Ongoing discussions with T45 indicate that substantial progress in process development has been made, and delivery of the remaining castings in late summer is anticipated. A status update briefing is scheduled after the latest round of casting trials is completed in mid June. Despite the defective castings, the lattice structure was sufficiently robust such that good structural performance was measured and model validation was accomplished.

2. Ligament Testing

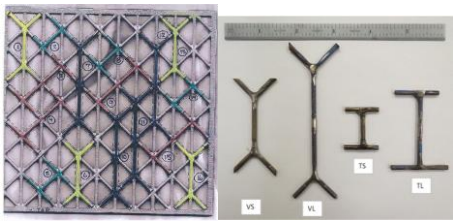

Fig. 2 *Ligament specimens*

Both 90° and 45° ligaments were machined from the Ti-6-4 and SMA lattice blocks in preparation for testing (Fig 2). Note that these test samples include lattice nodes, a likely site for casting defects. These unconventional geometries required a new gripping system to be designed in order to test in tension and compression. After several iterations, a clamping grip was devised and down-selected. Duplicate tension and compression tests of Ti-6-4 ligaments at 23, 165 and 200°C were completed, and representative stress-strain curves are shown in Figure 3a. In general, the measured strengths were only slightly lower than published data for conventionally processed materials, indicating that the casting process was producing acceptable microstructures. Some ligaments exhibited early failure, which is most likely due to casting defects. Obtaining crack-free tensile specimens from the SMA lattices has proven to be more difficult, so the only successful tests have been in compression, and compressive strains up to 15% were obtained without failure.

Ligament testing results were used as calibration data for the finite element modeling described below. In addition, the SMA specimen compressed at room temperature was subsequently heated to examine shape memory behavior. Approximately 3% strain was recovered upon heating, which is consistent with the expected behavior of the alloy. ***These tests successfully demonstrated shape memory behavior of the ligaments.***

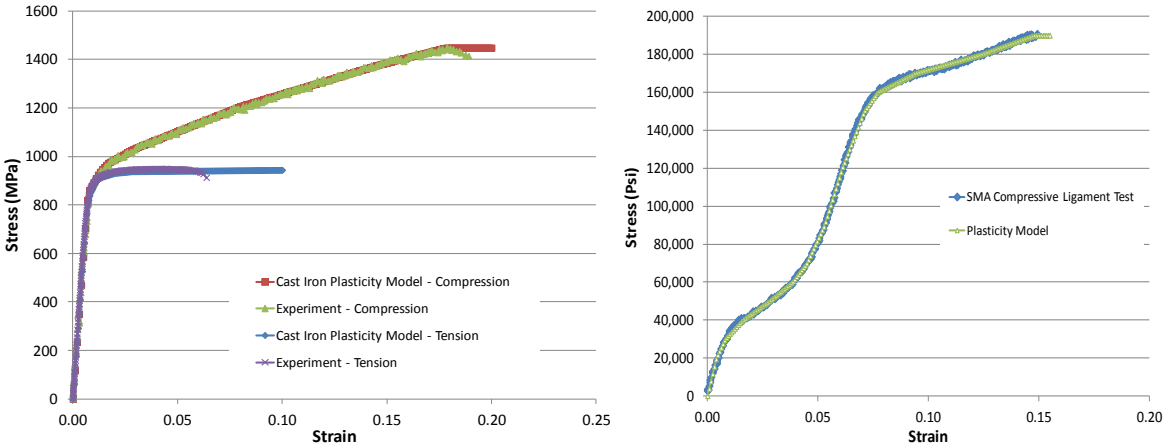

Fig. 3 *Ligament test results along with material calibration curve fits to existing Abaqus constitutive models. (a) Ti-6-4 in tension and compression. (b) SMA in compression.*

~~2~~3. Model development

The purpose of the modeling is to ensure a proper understanding of the physics of lattice deformation has been achieved, such that future extrapolations to new structures as well as optimization of the lattice structure can be performed with confidence. This will allow rapid, low cost evaluation of multiple structural concepts before investing in experimental demonstration efforts.

A Python script has been written to automatically generate Abaqus finite element models of ~~the~~ arbitrary lattice geometries. The script is parametric, so it is quick and easy to generate models for different configurations, run the finite element model, and post-process the results. The ligaments are treated as beams with arbitrary nonlinear material behavior that may also experience nonlinear geometric effects. Example lattice geometries generated using the Python script are shown in Fig. 4.

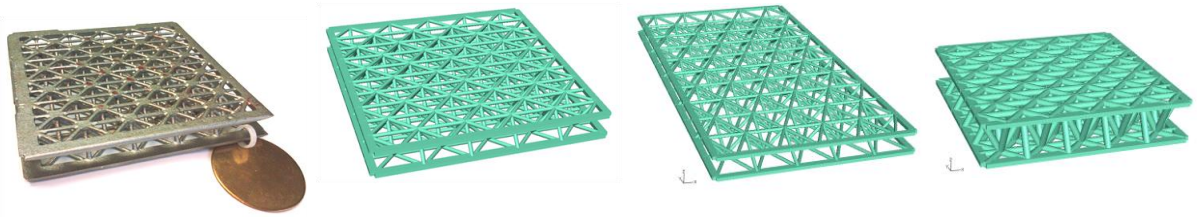

Fig. 4. *Actual lattice casting and sample geometries generated with the Python Script.*

The script has been specialized to generate models of the 4-point bend and flat-wise compression tests being conducted. The acreage ligament cross-section was treated as circular, while the edge ligament cross-section was treated as rectangular. Pre-test predictions, along with parametric sensitivity studies, were conducted for the 4-point bend configuration of the Ti-6-4 lattice. The 4-point bend test article and model geometry are shown in Fig. 5.

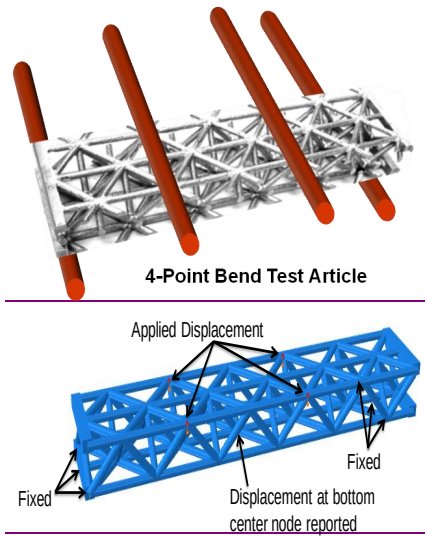

Fig.5 *4-point bend test article and finite element model*.

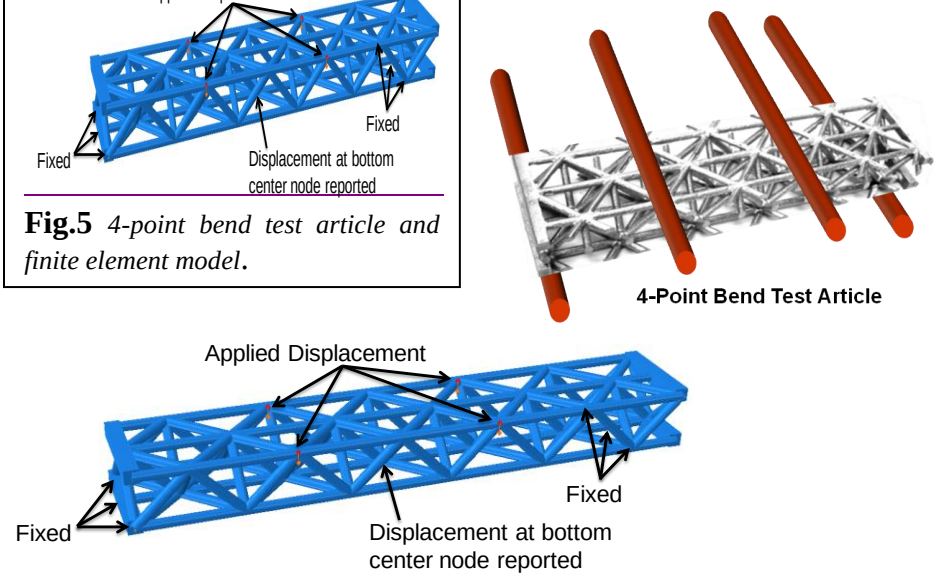

Fig. 5. *4-point bend test article and finite element model.*

After performing a mesh senstivity study to arrive at a globally converged mesh, a parametric sensitivity study was performed by varying the material representation, the height of the panel, and the ligament diameter. At the time of the pre-test predictions, only tensile ligament test results were available, and they showed some variability. The nonlinear material response was modeled using von Mises plasticity, and to capture the variability in the tensile test results, two sets of material data were used in the sensitivity studies, as shown in Fig. 6.

Variation of the panel height was intended to examine the effect of the fact that the ligament nodes in the as-built lattice are not centered at the center of the face ligements. This is shown in Fig. 7. To assess the impact of this offset, panel heights (distance between face ligament centroids) of 18 and 21.5 mm were examined.

Finally, ligament diameters of 3.25, 3.5, and 3.75 mm were examine to assess the impact of cross-sectional area variability, which has been observed in the lattice ligaments. The predicted applied load vs. bottom center point deflection is plotted in Fig. 8, along with deformation contours at various points. These two curves represented what what believed to be the best pre-test predictions, while still factoring in the variable Ti-6-4 material response as shown in Fig. 6. The predicted response involves a peak, followed by softening as the significant buckling of the top face struts is predicted. The model was loaded in diplacement control (on top face points, see Fig. 5) to a maximum of 4 mm, then unloaded. A significant amount of permanent set, due to plasticity, was predicted.

The full set of results from the parametric study, in which the panel height, Ti-6-4 material representation, and the ligament diameter were varied, are shown in Fig. 9. These results indicated that panel height and strut diameter have a significant effect on the lattice 4-point bend response (changes on the order of 35%), while the Ti-6-4 material variation examined is minor (changes on the order of 5%).

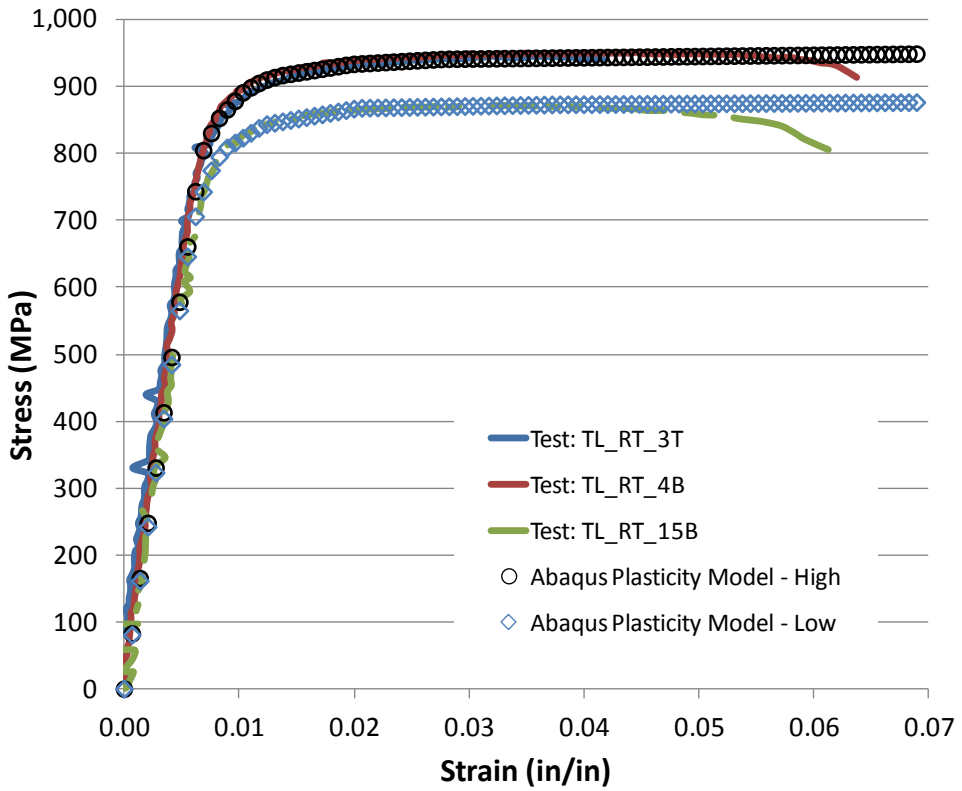

Fig. 6. *Abaqus plasticity model fit to room-temperature Ti-6-4 ligament test data that was used to capture the variability of the material response.*

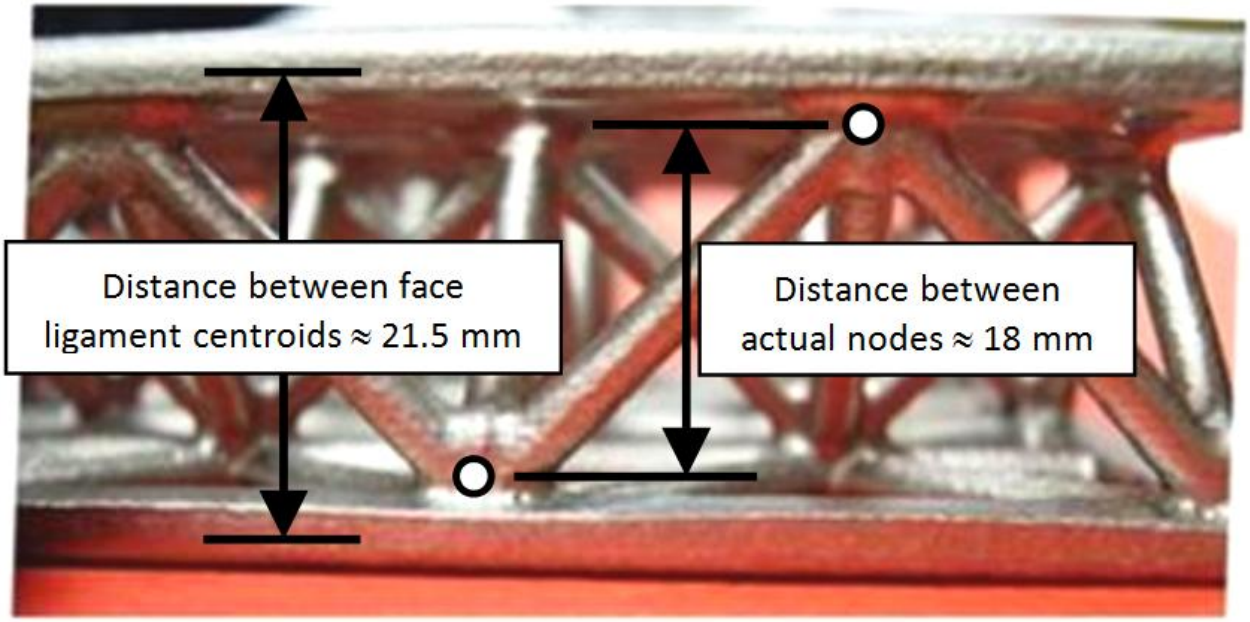

Fig. 7. Offset between face ligament centroids and actual node location.

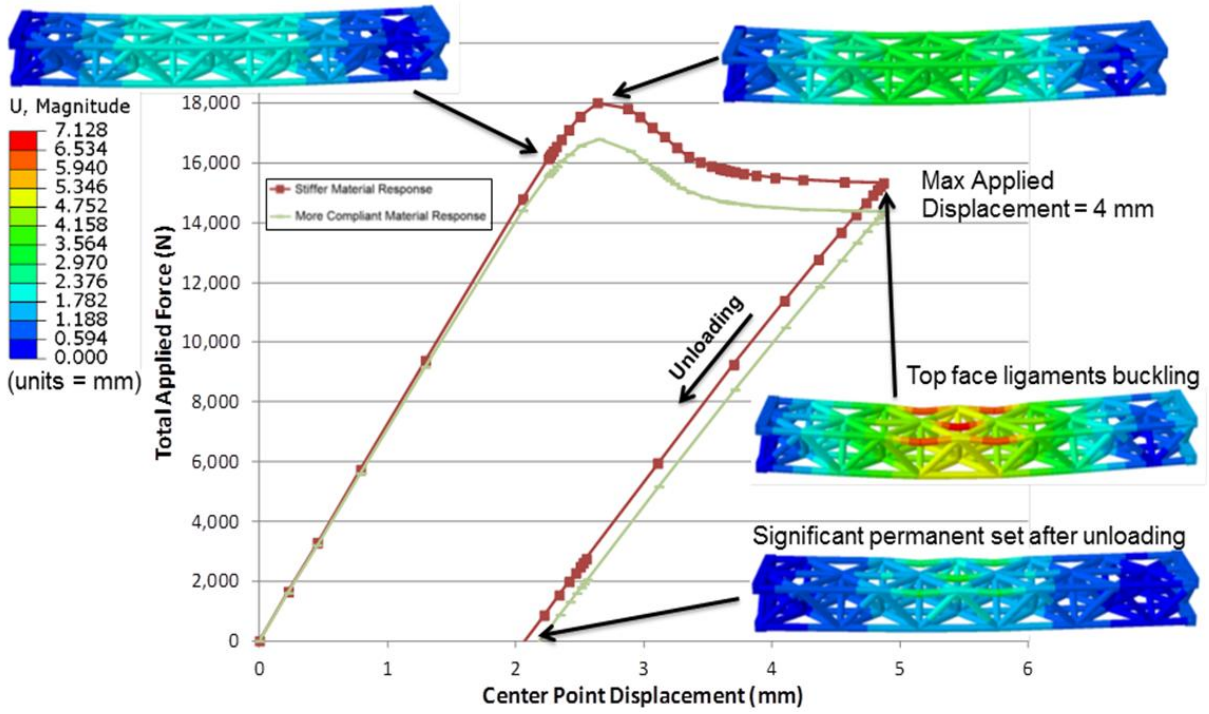

Fig. 8. *Pre-test prediction of Ti-6-4 lattice block 4-point bend response.*

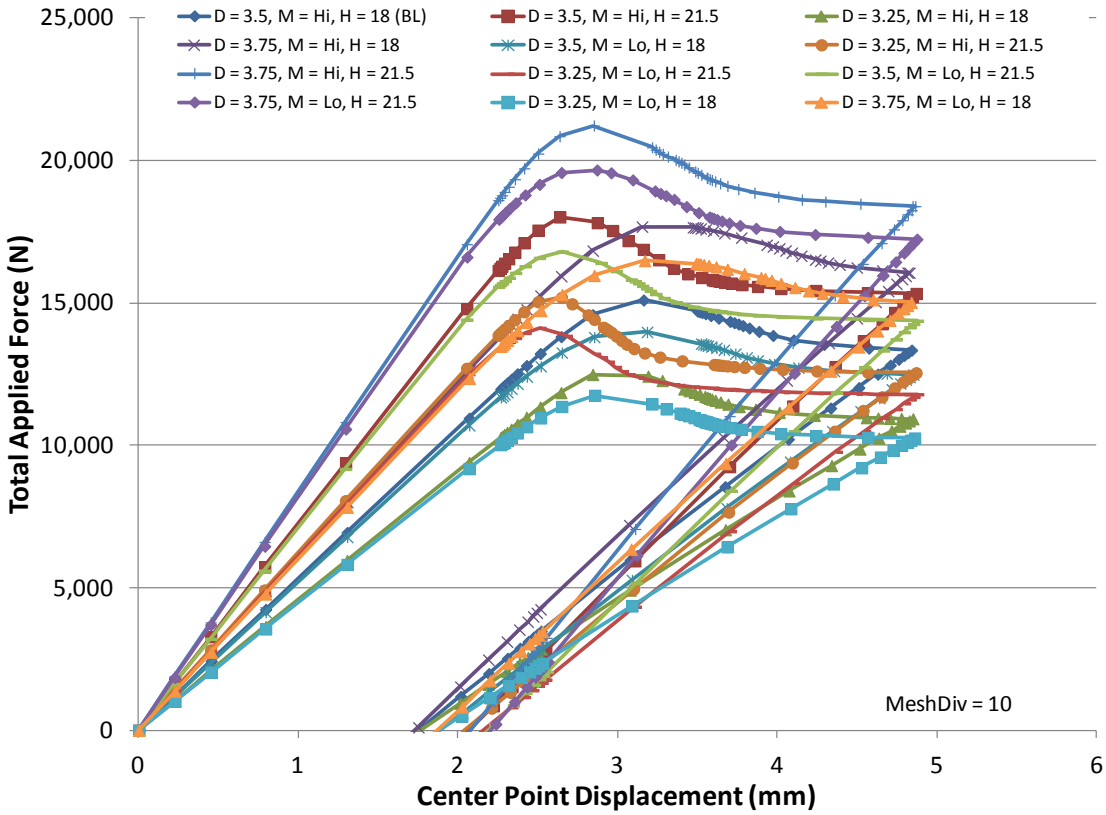

Fig. 9. *Full set of parametric simulations on the 4-point bend response of the Ti-6-4 Lattice.*

4. Structural Benchmark Testing

The Phase I structural benchmark testing effort included mechanical tests of complete lattice structure test articles. By evaluating the mechanical response to prototypical structural loadings, this work provided physical evidence of advantages in the lattice structure configuration, highlighting light weight, efficiency, and redundancy in the cellular structure. In addition, the testing demonstrated shape memory response in a lattice structure, as opposed to the simple geometry of a material test coupon. As described in the next section, the tests also provided data for verification of the soundness of the model development effort.

The structural benchmark test plan for Phase I included a variety of mechanical tests on similarly configured lattice structure test articles fabricated both from a cast lightweight aerospace titanium alloy (Ti-6-4) and from a cast SMA (NiTi). The planned testing provided for structural response evaluation at room temperature and at elevated temperature (165 °C) for "long-beam" bend tests with four-point loading, and for through-thickness flat-wise compression load tests. Due to the previously described delays in receiving acceptable test articles, benchmark testing was restricted to 1) demonstrate preparation for and validity of the two test methodologies; and, 2) provide initial test results for three test articles in two configurations fabricated from the two cast alloys.

Lattice structures cast in Ti-6-4 were received in two configurations: 100 x 100 x 25 mm panels, and a 50 x 200 x 25 mm panel. The former were retained for future flat-wise compression testing, while the latter was cut into three long-beam bending test articles. Lattice structures cast in the SMA NiTi were also received, in the 100 x 100 x 25 mm panel configuration, suitable for flat-wise compression tests. All castings exhibited visible defects, including porosity and cracks at nodes and struts.

Structural Benchmark Testing Accomplishments

The structural benchmark testing accomplishments include contributions to Phase I Products by providing mechanical test properties and shape memory test data for lattice block structures made from SMA and Ti-6-4, and by providing structural response data that was used for validation of the finite element-based deformation model. These contributions are further described in the following paragraphs. Note that castings in the auxetic structure configuration were not available in this time period for reasons previously described.

The Phase I Task 1 objective to prepare for testing was met by acquiring test fixtures, instrumentation, and furnace/heating hardware, and by preparing the mechanical test rigs and data acquisition systems to perform structural benchmark testing. Task 2 was not applicable to structural benchmark testing. The Task 3 objective to perform isothermal testing was accomplished for test articles fabricated from conventional lattice castings of both Ti-6-4 and SMA (note again that the auxetic structure configuration was not available in this time period). The Task 4 objective to demonstrate strain recovery through thermal treatment was accomplished by loading two SMA lattice structures to significant strain levels in flat-wise compression; in the first case, the structure fractured in the process due to pre-existing casting defects, so strain recovery was not consequential and therefore not attempted. In the second case, the SMA test article was loaded to result in 2% permanent structural strain, 60% of which was recovered following heat treatment. Further description of the testing is included in the following paragraphs. The Task 5 objective to prepare a final report is satisfied by completion of this manuscript.

Structural Benchmark Testing Description and Results

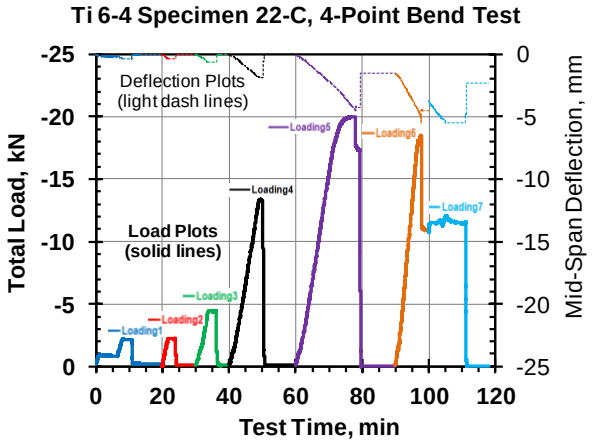

Figure 11. Bend test load ramps. *A series of bend test load ramps were applied to the lattice structure beam.*

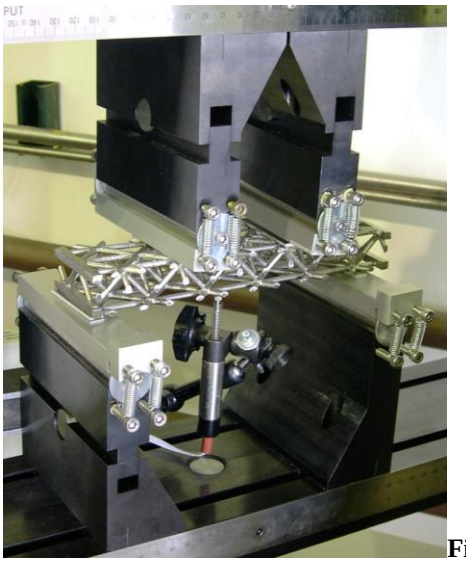

Figure 10. Long-beam bend test set-up. *Lattice structure test article is shown mounted in hinged four-point load fixtures.*

Three series of structural benchmark tests were completed: 1) long-beam bend (four-point load) testing of a cast Ti-6-4 lattice structure; 2) flat-wise compression strength testing of a cast SMA NiTi lattice structure; and, 3) flat-wise compression yield of a cast SMA NiTi lattice structure testing with thermal recovery. All test series were conducted isothermally at room temperature (22 °C).

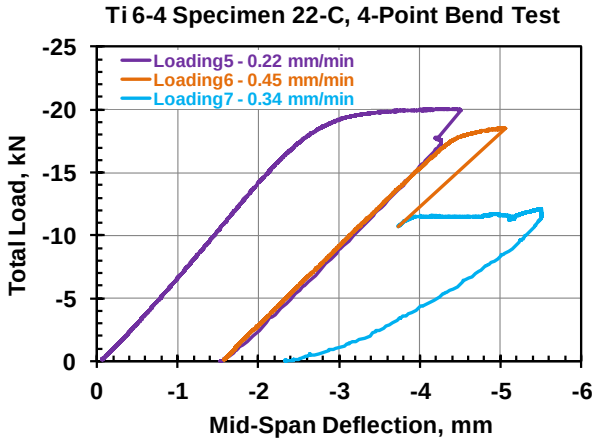

Figure 12. Failure and residual strength tests. *After first failure, most lattice structure strength remained.*

The first test series was performed on Ti-6-4 Test Article S/N 22C; it had overall dimensions of 200 x 50 x 25 mm and was 12 by 3 unit cells, composing three longitudinal "trusses." The average strut diameter was 3.505 mm. The long-beam bend test configuration (Fig. 10) of the 50 kN MTS load frame was symmetrical, with lower reaction supports at two-node locations spaced 180 mm apart, and upper load rollers also at two-node locations spaced 72 mm apart. Four-point loading placed the entire middle span between load rollers under the same maximum nominal moment value. In bending, the test article's structural limits were explored through a series of increasing load ramp cycles (Fig. 11). Elastic loadings to 2.224 kN, 4.448 kN, and 13.34 kN total load were completed with almost no measurable nonlinearity or hysteresis upon return to zero load. The elastic series was followed by loading to first observed strut failure at 20.01 kN; the response remained quite linear until approximately 18 kN. Specimen inspection using optical microscopy could not locate the suspected fracture. Additional residual strength testing was continued under test machine stroke control, when 18.49 kN strength was measured at second strut failure. Residual strength of 12 kN was observed until the machine stroke limit of 5.5 mm specimen deflection was reached (Fig. 12). Post-test visual inspection revealed two fractures, one at a node and one through a strut.

Figure 13. Flat-wise compression test. *Lattice structure test article is shown mounted between platens, with spherical joint fixture beneath specimen.*

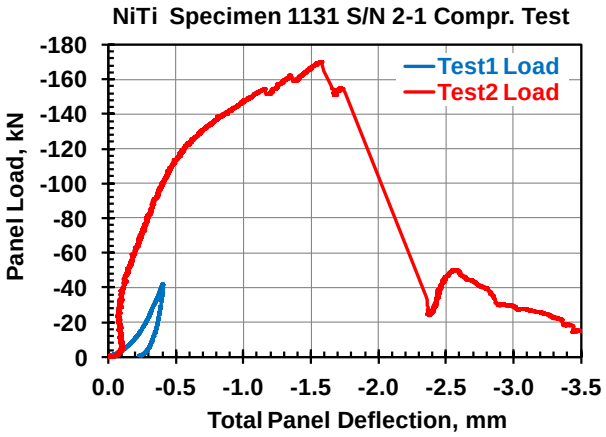

Figure 14. Compression strength test. *Additional strength and deformation were available after the initial break of the first SMA test article at 155 kN.*

The second test series was performed on SMA NiTi Test Article Heat 1131 S/N 2-1; it had overall dimensions of 98 x 99 x 26 mm and was five unit cells square. The average strut diameter was 3.858 mm. The flat-wise compression strength test was performed first on the 50 kN MTS load frame and included a spherical joint fixture and rigid platens to assure uniform loading of all 18 upper and 18 lower "face sheet" nodes (Fig. 13). In compression, the test frame's load limit was approached prior to significant deformation or failure of the test article; a peak loading of 41.9 kN was recorded at 0.41 mm panel deflection. To further explore the load-carrying ability of the SMA test article, a 450 kN-capacity Instron load frame was reconfigured with the spherical joint and platen fixtures. Upon loading, first failure was identified at 155 kN total panel load; in situ inspection revealed a crack in the specimen's integrally cast lower perimeter tension frame, probably at a pre-existing flaw. Continued higher loading under stroke control demonstrated load redistribution capability within the lattice structure, providing additional strength to achieve the peak load of 170 kN at 1.6 mm deflection, approximately 6% structural through-thickness deformation (Fig. 14). Post-test visual inspection revealed additional cracks in the upper and lower perimeter tension frames. This altered the structure's stress distribution, placing struts in bending and progressively failing most nodes and cracking many struts at mid-length locations. Because of the extensive non-reversible damage, post-test thermal treatment for strain recovery (self-healing) was not warranted.

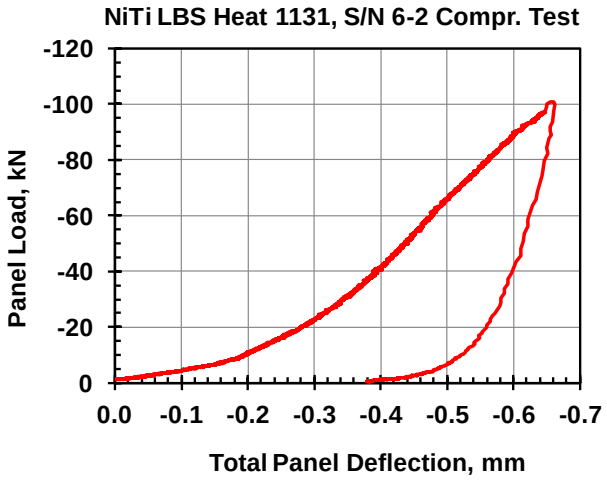

Figure 15. Compression yield test. *The second SMA lattice structure test article was loaded in compression to produce approximately 2% residual deformation.*

The third test series was performed on SMA NiTi Test Article Heat 1131 S/N 6-2; it had the same overall dimensions and geometry as Test Article S/N 2-1. The flat-wise compression yield test with strain recovery was performed on the 450 kN-capacity Instron load frame configured with the spherical joint and platen fixtures (similar to Fig. 13). In compression at a rate of 0.305 mm per minute, a peak load of 101 kN was attained at a deflection of 0.65 mm, equivalent to 3.1% compressive structural strain (Fig. 15). No evidence of cracking or failure of the structure was observed. Following release of the load, the residual compressive through-thickness strain was 1.95%; this value relaxed to 1.58% after a period of 15 minutes at room temperature. Post-test heat treatment at 95 °C resulted in strain recovery to 1.33%, while an additional heat treatment at 200 °C for 120 minutes produced strain recovery to 0.79% -- 60% of the initial inelastic deformation after release of the load (Fig. 16).

Structural Benchmark Testing Conclusions

In general, familiarity with the lattice structure test articles revealed that the large surface area and configuration of the cellular casting make difficult non-destructive inspection for determining the presence of all cracks and defects.

The long-beam bend testing of a Ti-6-4 lattice structure exhibited almost no inelastic behavior for loadings to 13.34 kN, indicating that yield at local stress risers if it existed did not affect the overall structural response. After the first and second tensile failures of a strut (or node), much strength and deformation capability existed, demonstrating the advantages of the highly redundant lattice structure, with resilience and availability of alternative load paths. In bending, the top compression struts plastically deformed before the first bottom strut tensile rupture was discovered. For aerospace service, this is a valuable benefit, because it provides an observable sign of distress before structural failure. Necking deformation at strut tensile breaks indicates fully developed plasticity above the Ti-6-4 material's yield point. As a testing consideration, large specimen deformations observed require careful selection of the appropriate load and support fixtures to permit free rotations and lateral movements.

Flat-wise compression testing of SMA NiTi lattice structures indicated insensitivity to defects for this load case; the test articles had several known casting defects present, but until failure of the integral tensile frame in one case, the defects did not affect test results to a measurable degree. The initial 0.2 mm

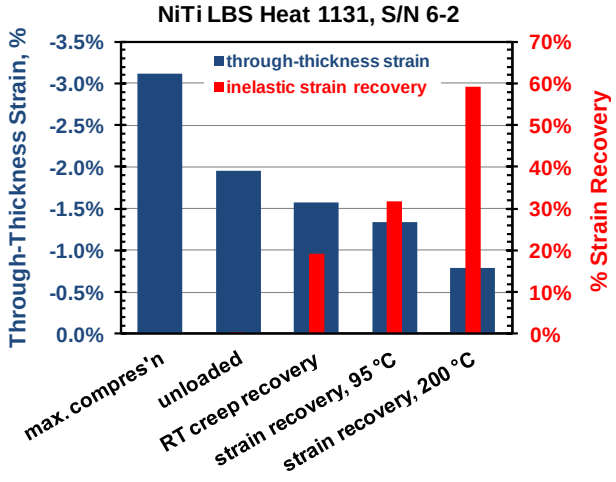

Figure 16. Recovery of compressive strain. *Thermal treatment restored 60% of the initial inelastic strain resulting from extreme compression of the test article.*

unrecovered deformation of the first compression test article upon unloading from the first cycle to 41.9 kN total load may have resulted from local yielding, as the node outer contact surfaces on the as-received casting were not milled to provide a planar surface, or from general inelastic behavior. In the former case, non-uniform loading would develop at the nodes when first contacting the rigid platens' flat surfaces. Similarly, this may be responsible for the condition of initial increasing stiffness with load during the compression tests. For the first compression test article, upon second loading the compliance to 41.9 kN was greatly different than for the first cycle, a behavior unique and characteristic of the SMA material. For the second compression test article, the recovery of 60% of the initial inelastic strain through heat treatment is representative of the shape memory alloy. Further, upon subsequent repeated load cycling, nearly all inelastic strain is expected to be recoverable through heat treatment, an advantageous property of the NiTi alloy composition. Finally, the high value of structural deformation at peak strength load capacity of the SMA test article further indicates an opportunity for high strain recovery (self-healing) upon thermal treatment.

5. Analytical Verification

The agreement between the most representative pre-test prediction and the bend test performed on the Ti-6-4 lattice is shown in Fig. 17. As shown, the model predicts the inital slope and onset of nonlinearity well, but the softening associated with top ligament buckling is absent in the test data. In the test, failure occurred in one of the two ligaments in the bottom face as shown. Note that no attempt to model this type of ligament fracture has yet been made. The lack of softening in the test results indicates that buckling of the top face struts was limited in the test and overpredicted in the model.

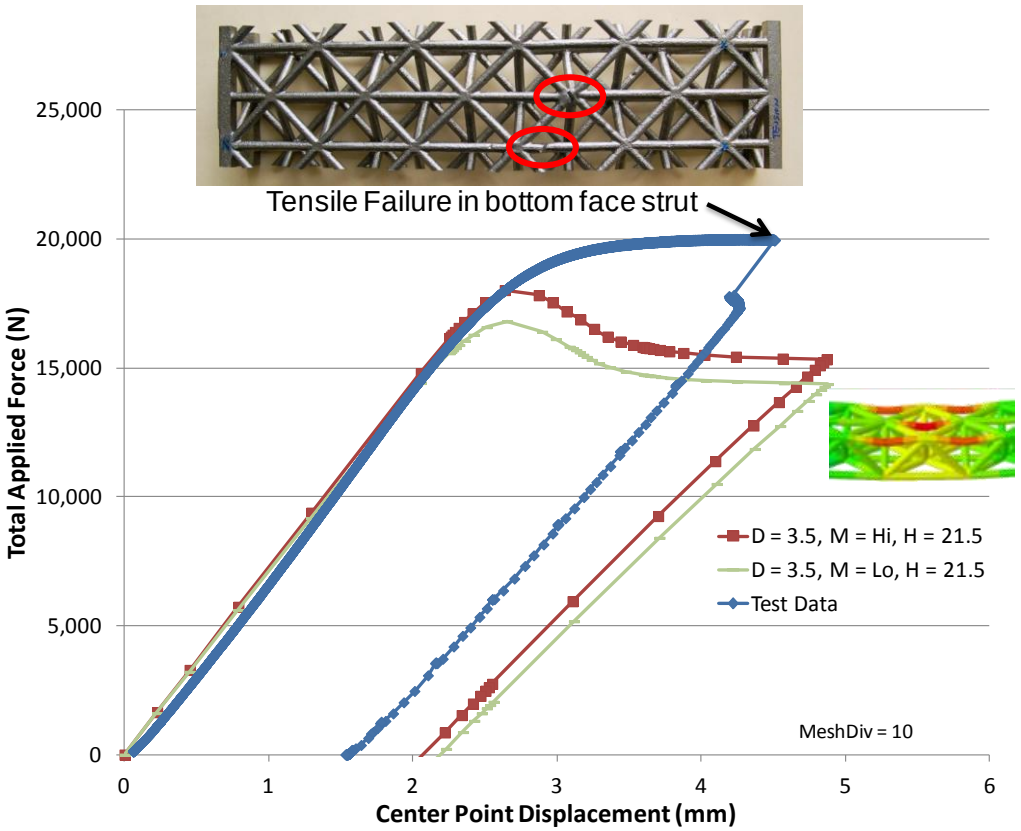

Fig. 17. *Correlation between pre-test prediction and Ti-6-4 LBS 4-point bend test data.*

In an attempt to explain the discrepancy, compressive ligament test data, which became available after the 4-point bend test, was modeled using an existing model in the Abaqus library ("cast iron plasticity model"), which allows distinct tensile and compressive material plastic behavior. The fit of the model to experimental room-temperature Ti-6-4 ligament data is shown in Fig. 3a, where now the compressive response is hardens significantly more than the tensile response. Switching to this material model decreased but did not eliminate the amount of softening in the model (see Fig. 18). To further suppress the buckling in the top face ligaments, a non-circular ligament cross-section was considered in the top face of the lattice only. This simulates the tear-drop shaped cross-section that has been observed (see Fig. 18) and enables the ligaments to have greater resistance to out-of-plane bending and thus greater buckling resistance. For simplicity, a rectangular cross-section was considered as shown in Fig. 18.

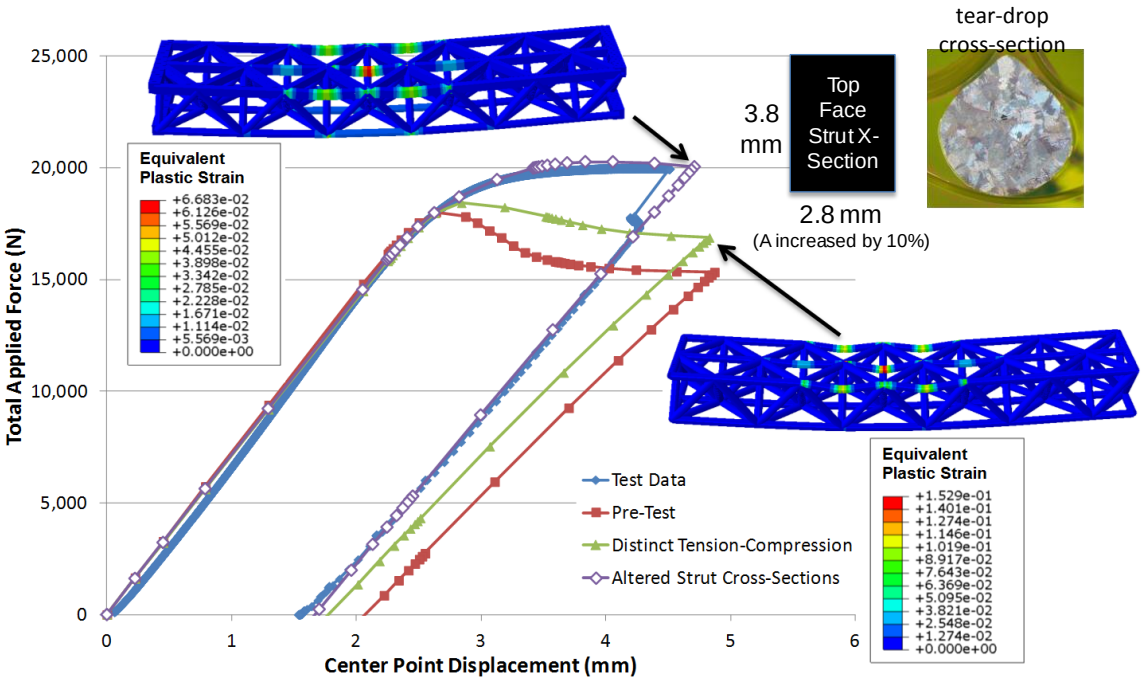

Fig. 18. Correlation of m*odel, altered to suppress top face ligament buckling, with experiment for the Ti-6-4 lattice 4-point bend test.*

Fig. 18 compares the altered model with the experimental data. While the rectangular shape of the top face ligaments is not completely representative, this simulation shows that by suppressing buckling of the top face ligaments, the test data can be captured. An additional feature that will also suppress top face ligament buckling is the thicker ligament sections near the nodes, which was not included in the model geometry. This reduces the free-span of the ligaments, which will reduce their tendency to buckle. This effect will be examined in the future.

Finally, a pre-test prediction was made for the flat-wise compression behavior of the SMA lattice. The actual casting and the Abaqus model are shown in Fig. 19. To simulate the flat-wise compression test, the bottom nodes in the model were fixed and the top nodes were displaced downward at a constant rate. As a first step, the SMA material was modeled using the Abaqus von

Mises plasticity constitutive model. The fit of this model to SMA ligament tensile test data is shown in Fig. 3b. More realistic SMA constitutive models will be employed in the future. The agreement between the pre-test flat-wise compression prediction and experiment is shown in Fig. 20. The model matches the experiment well for the initial slope and onset of nonlinearity. The model is then slightly more compliant than the test data. The model response begins to stiffen in association with the SMA material stiffening response shown in Fig. 3b. The model then was not able to converge due to the extensive buckling of the lattice internal ligaments. Although this cannot necessarily be considered a predicted failure, it did occur at an applied displacement of 1.18 mm, which corresponds closely to the applied displacement at first failure in the test (1.16 mm).

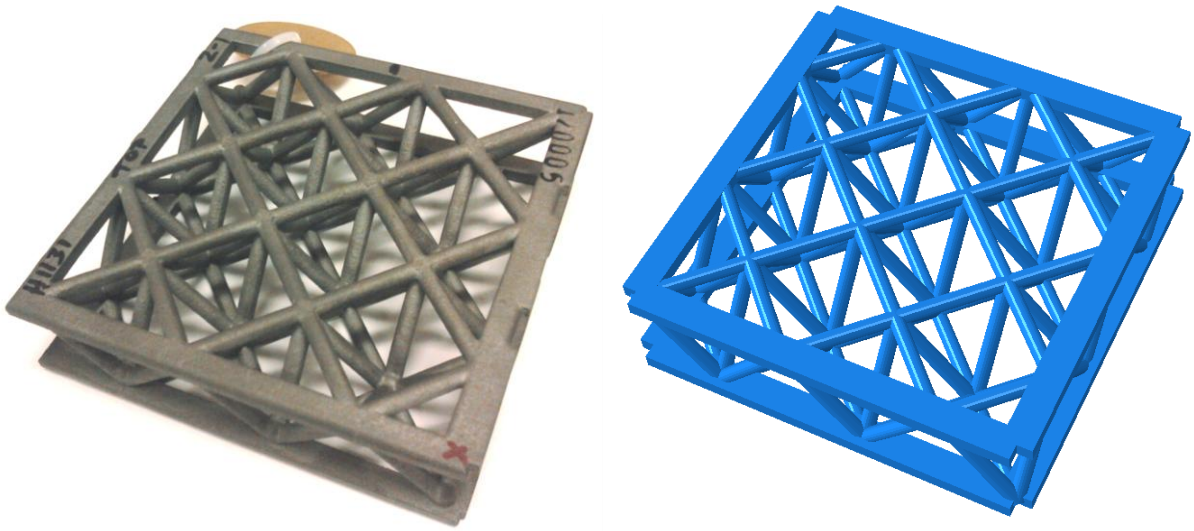

Fig. 19. *SMA lattice casting and Abaqus finite element model.*

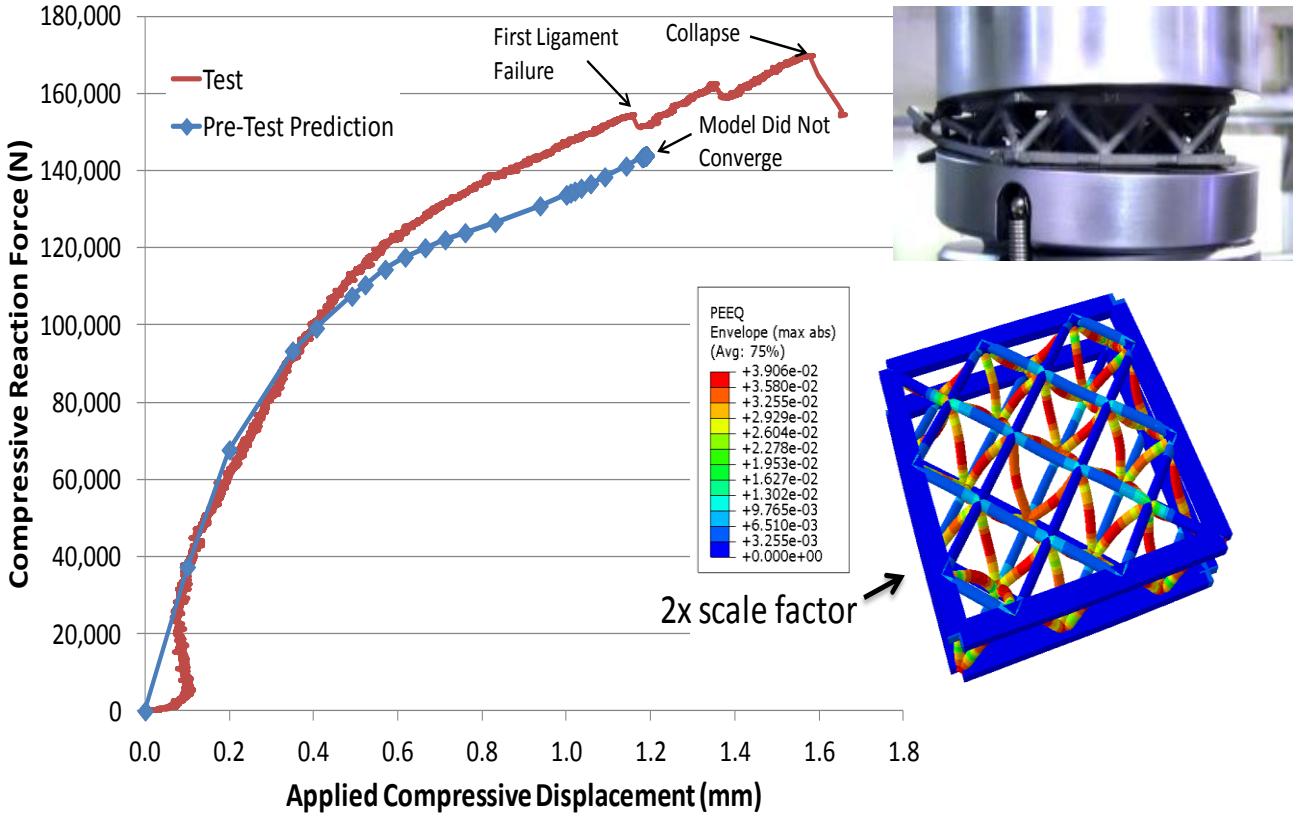

Fig. 20. *Model prediction and experimental results for SMA lattice in compression.*